Thermally Controlled Onset of Spatially Incoherent Emission in a Broad-Area Vertical-Cavity Surface-Emitting Laser

Gordon Craggs, Guy Verschaffelt, *Member, IEEE*, Shyam K. Mandre, Hugo Thienpont, *Member, IEEE*, and Ingo Fischer

***Abstract*—We present an experimental study of the physical process that leads to spatially incoherent, nonmodal emission in broad-area vertical-cavity surface-emitting lasers. We show that this special emission regime that occurs in pulsed operation of these lasers is due to a combination of a spatially distributed thermal or refractive index gradient (thermal lens) and thermal expansion of the cavity during the pulse (thermal chirp). Our measurements are based on preinstalling a thermal lens through a current bias, and subsequently, modulating a pulse onto the bias. This approach allows us to independently investigate the role of both thermal effects in the onset of nonmodal emission.**

***Index Terms*—Semiconductor laser, spatial coherence, thermal effects, vertical-cavity surface-emitting laser (VCSEL).**

I. Introduction

VERTICAL-cavity surface-emitting lasers (VCSELs) are popular commercial semiconductor lasers due to the fact that they are able to provide a single-mode circular beam at low cost [1]–[3]. They can be found in a number of applications in the field of optical data communication [4], [5] and sensing [6]–[8]. In order to obtain such a high-quality beam from a monolithic VCSEL, it is, however, necessary to restrict the transverse size of the cavity to a few micrometers. The small transverse size will limit the available output power to a few milliwatts typically [9], [10]. This low output power level can be disadvantageous for a number of applications such as illumination, projection, and printing. A high-power and high-quality beam can be achieved by using a vertical external cavity configuration (VECSEL) [11]. For a monolithic cavity design, the output power can easily be raised by increasing the transverse size of the cavity [12], but at the expense of a much reduced beam quality: because of the large Fresnel number of such broad-area VCSELs (BA-VCSEL) multiple competing transverse modes will be emitted [13], [14].

Manuscript received October 31, 2008; revised February 6, 2009. First published April 21, 2009; current version published June 5, 2009. This work was supported by the IAP P6/10 network "Photonics@be" and the Vrije Universiteit Brussel-Industrieel OnderzoeksFonds (VUB-IOF) project "Micro-photonics."

G. Craggs, G. Verschaffelt, and H. Thienpont are with the Department of Applied Physics and Photonics, Vrije Universiteit Brussel (VUB), Brussels 1050, Belgium (e-mail: gordon.craggs@vub.ac.be; guy.verschaffelt@vub.ac.be; hthienpo@vub.ac.be).

S. K. Mandre was with the Institute of Applied Physics, Darmstadt University of Technology, Darmstadt D-64289, Germany. He is now with Braun GmbH, Kronberg 61476, Germany (e-mail: shyammandre@googlemail.com).

I. Fischer is with the Joint Research Institute of Integrated Systems and School of Engineering and Physical Sciences, Heriot-Watt University, Edinburgh EH14 4AS, U.K. (e-mail: laserdynamics@gmail.com).

Digital Object Identifier 10.1109/JSTQE.2009.2016355

In principle, semiconductor lasers are coherent light sources. However, we have shown in [15] and [16] that BA-VCSELs can be driven into a regime of nonmodal, spatially incoherent emission by injecting these devices with appropriate current pulses. In this regime, the VCSEL can be described as a quasi-homogeneous Schell-model source [17], [18]. This special regime has proven to be attractive for applications, as it has a positive influence on the speckle contrast in a projected image [19]. The spatially incoherent emission regime also has a positive consequence for the laser's beam shape: the emission in higher order transverse modes changes into emission in local coherence islands. This results in a Gaussian intensity profile in the VCSEL's far field (FF). The observed loss of spatial coherence is neither accompanied by any noticeable reduction of the output power, nor by any fast fluctuations of the output intensity [16]. The nonmodal emission regime occurs for pulse durations between one and several tens of microseconds, which corresponds to the typical timescale for thermal effects in VCSELs [20], [21]. These observations indicate that the destruction of the modal structure in the FF is caused by thermal effects. More specifically, we think two phenomena play a joint role: thermal chirp (expansion of the laser cavity) in combination with a thermal lens (build up of a transverse thermal, and thus, refractive index profile). Both thermal effects are due to heating of the cavity induced by the injected current, but they might play a different part in leading up to spatially incoherent emission. As the thermal lens increases in strength, we suspect that the time required for the build up of the coherence of a particular mode pattern increases. Once this "modal coherence buildup time" (MCBT) is sufficiently large, the thermal chirp can keep the laser cavity in a transient state, such that modal coherence does not emerge. As a result, the laser remains in a state of nonmodal, spatially incoherent emission. This hypothesis might explain why we observe the spatially incoherent emission regime in a BA-VCSEL only several hundreds of nanoseconds after the onset of laser emission: this delay is determined by the time needed for a sufficiently strong thermal lens to build up in the laser cavity.

The novelty presented in this paper consists of investigating the respective contributions of the thermal lens and thermal chirp, thus providing more insight into their joint effect that leads to nonmodal emission. We do this by conducting an experimental analysis based on the different timescales at which both effects take place. The technique used throughout the analysis relies on the preinstallation of a thermal lens before the

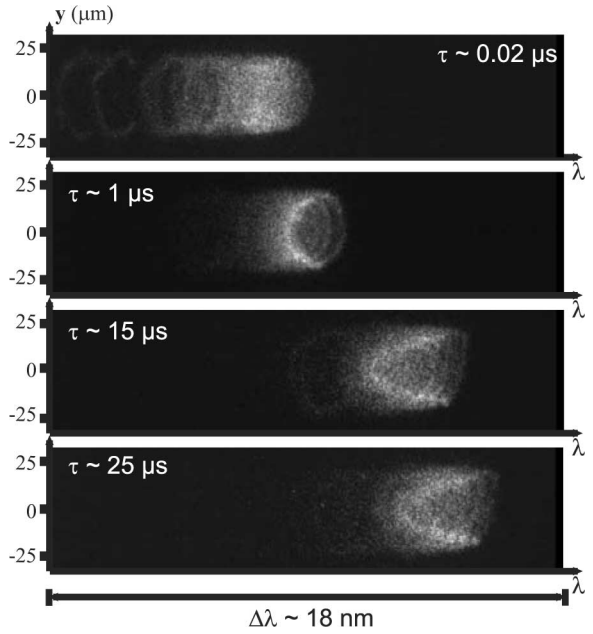

Fig. 1. Sequence of single-shot measurements of the BA-VCSEL's spectrally dispersed NF emission behavior. The ordinate indicates the spatial position y in the NF with respect to the VCSEL's center. The abscissa depicts both the spatial direction x and spectral information. The BA-VCSEL was driven by 30 μs long pulses with an amplitude of 160 mA. The times denoted in the corner of the images are the positions of the single-shot measurements after turn-ON.

current pulses are applied. We achieve this by means of a bias current.

II. Device Characteristics

In our measurements, we use an oxide-confined BA-VCSEL with an aperture radius R of 25 μm, similar to the device used in [15]. The BA-VCSEL emits at wavelengths around $\sim$840 nm, with a maximum cw output power of $\sim$ 70 mW at an injected current of 80 mA. The VCSEL's threshold current is approximately 14 mA. The pulse conditions required in order to induce the nonmodal, incoherent emission regime are described in [15].

III. Thermal Lens and Chirp

As stated before, we expect that both the thermal lens and the thermal chirp play a distinct role in generating the nonmodal emission regime. Therefore, we first quantify these thermal properties for our VCSEL using the setup from [22]. In this setup, the BA-VCSEL's near field (NF) is imaged onto the input slit of a 1 m Czerny–Turner imaging spectrometer. The spectrally dispersed NF profile is then imaged onto a fast-gated intensified CCD Camera (iCCD, *4Picos, Stanford Computer Optics Inc.*) with an exposure time of 300 ps. In Fig. 1, we show a few examples of such obtained measurements of the VCSEL's spectrally dispersed NF for different times τ after turn-ON of the laser and an injected current of 160 mA. These images provide spatial resolution of the NF along the ordinate and the abscissa and additional spectral dispersion of the NF along the abscissa. This experimental technique has the advantage of providing 2-D spatial resolution with additional spectral resolution along the abscissa.

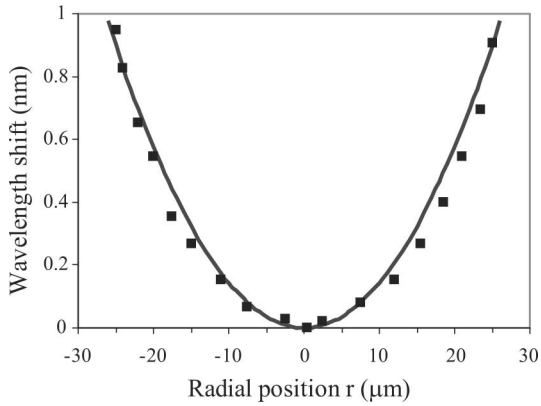

Fig. 2. Radial wavelength shift relative to the wavelength in the center of the BA-VCSEL for 1 μs pulses with an amplitude of 160 mA (squares) and comparison to a parabolic fit (full line).

A few nanoseconds after turn-ON of the laser, the VCSEL exhibits modal emission. The spectrum (see measurement at τ equal to 0.02 μs in Fig. 1) contains faint rings corresponding to high-order transverse modes on the short-wavelength side of the spectrum and a cloud of modes that cannot be resolved on the long-wavelength side. A few hundreds of nanoseconds after laser turn-ON, the nonmodal emission regime is reached. In this regime, the high-order modes disappear and the spectrum transforms into a parabola-like structure (see spectra in Fig. 1 for τ equal to 1, 15, and 25 μs). Light is now emitted in independent coherence islands and the wavelength of each of these coherence islands is determined by the local cavity conditions, i.e., the optical resonator length at the position of the individual coherence islands. The curved structure of the spectrum thus indicates that the resonator length is not constant across the VCSEL's aperture. The parabola-like shape of the spectrum is therefore direct evidence of the VCSEL's thermal lens. From the spectra in Fig. 1, we can deduce the spatially resolved wavelength shift [22], as shown in Fig. 2, for a pulse amplitude of 160 mA and length of 1 μs. The thermal lens $\Delta\lambda_{\mathrm{lens}}$ within the cavity can be well-described by a parabola, i.e., $\Delta\lambda_{\mathrm{lens}} = B\, r^2/R^2$, where R is the VCSEL's aperture radius and B is 0.85nm for a pulse amplitude of 160 mA.

The strength of the thermal lens is determined by the width of the parabola in Fig. 1, or equivalently by the wavelength shift B in Fig. 2 between the center and the edge of the VCSEL. By measuring the spectrally dispersed NF for different pulse durations, we can reconstruct the evolution of the thermal lens. This result is shown in Fig. 3, where we plot the width B of the parabola-shaped spectrum for different times τ after laser turn-ON. The spectral width of the parabola initially increases but then saturates after $\approx$7 μs. The evolution of the spectral width can be approximated by an exponential dependence $B = A\ (1 - \exp(t/\tau_{\mathrm{lens}}))$, where τ_{lens} is the time constant of the build up of the thermal lens and A is a scaling factor. Of course, the strength of the thermal lens will also depend on the power dissipation P_{diss} in the VCSEL. If we assume this dependence

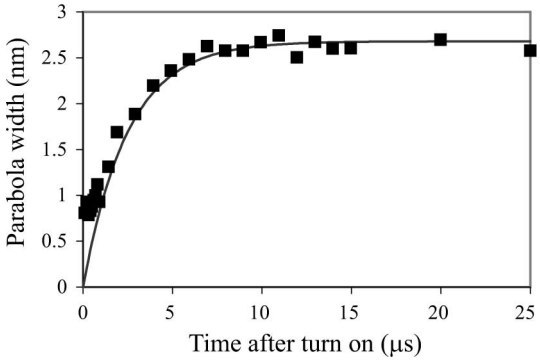

Fig. 3. Evolution of the width B of the parabolic spectrum at 160 mA and fit to an exponential function as described by (1) (full line).

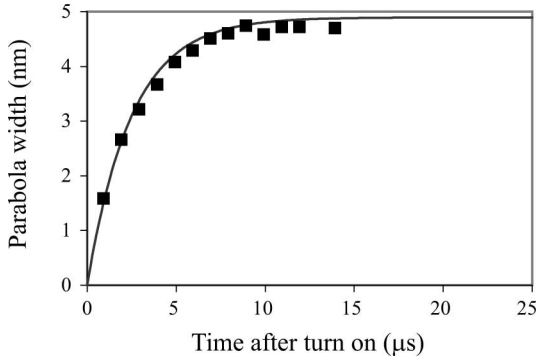

Fig. 4. Evolution of the width B of the parabolic spectrum at 200 mA and fit to an exponential function as described by (1) (full line).

to be linear, we can determine the strength of the thermal lens for any pulse duration and amplitude via

$$B = A\ (1 - \exp(t/\tau_{\rm lens}))\ P_{\rm diss} \tag{1}$$

The power dissipation depends on the injected current I through

$$P_{\rm diss} = \eta_S I_{\rm th} + (V_{\rm th} - \eta_S)\ I + R_d I^2 \tag{2}$$

where η_S is the slope efficiency $(0.8\,{\rm W/A})$, $I_{\rm th}$ is the VCSEL's threshold current $(14\,{\rm mA})$, $V_{\rm th}$ is the threshold voltage $(1.58\,{\rm V})$, and R_d is the VCSEL's differential resistance (in ohms). We have fitted the data of Fig. 3 onto such an exponential dependence, yielding a value for $\tau_{\rm lens}$ of 2.5 μs and for the scaling factor A of $6.8 \times 10^{-3}\,{\rm nm/mW}$.

In order to check the validity of (1) for other pulse parameters, we have measured the evolution of the spectral width B for a pulse amplitude of $200\,{\rm mA}$. The result of this measurement is shown in Fig. 4. In this figure, we have also plotted the evolution of B, as described by (1). We find a good agreement between the model and the measured values of B for a value of the scaling factor A of $8.5 \times 10^{-3}\,{\rm nm/mW}$. This is about 20% larger than for the measurement at an injected current of 160 mA and indicates that the thermal lens strength scales slightly superlinear with respect to the dissipated power.

The spectra in Fig. 1 also reveal a shift of the emission toward longer wavelengths during the pulse due to Joule heating. Fig. 5 depicts the average wavelength shift during a 25-μs-long pulse. The chirp or average wavelength at each temporal position is calculated as the intensity-weighted average over the corresponding single-shot spectrum of Fig. 1. Fig. 5 shows that the emission wavelength shifts more than 6 nm within the first 25 μs of emission. The wavelength shift $\Delta\lambda_{\rm chirp}$ can be approximated by a power law

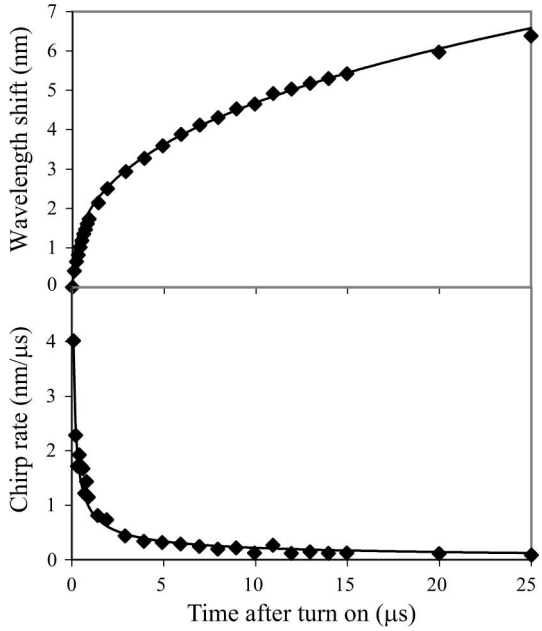

Fig. 5. Thermal chirp and chirp rate for a pulse amplitude of 160 mA and fit (full line).

$$\Delta\lambda_{\rm chirp} = m\ t_{\text{turn-ON}}^{b}\ P_{\rm diss} \tag{3}$$

where m is a scaling factor and the fitted value of b is 0.37. From the measurement of the thermal chirp, we can directly derive the chirp rate, which is the speed at which the cavity resonance changes in time. The chirp rate is also shown in Fig. 5. The thermal chirp rate is clearly the largest at the beginning of the pulse, whereas the thermal lens requires a few microseconds to build up completely. We will use this separation of timescales in order to independently investigate the role that both thermal effects play in the onset of nonmodal emission.

IV. Effect of the Thermal Lens

A. Measurement Procedure: Gaussian FF as Indicator

In order to quantify the VCSEL's spatial coherence properties, we need to measure the complex degree of coherence [17]. This can, e.g., be done using a reversing wavefront interferometer [23], but this measurement procedure is time-consuming. Nevertheless, we have observed and explained that the spatially incoherent emission of the studied BA-VCSEL always coincides with an apparent Gaussian intensity distribution in the VCSEL's FF [15]. In case of modal emission, the BA-VCSEL emits multiple higher order Laguerre modes that results in a structured FF with a minimum in the center of the FF intensity profile. We can thus consider the appearance of a Gaussian-shaped FF as a measure for the destruction of spatial coherence, which is much easier than determining the full coherence function.

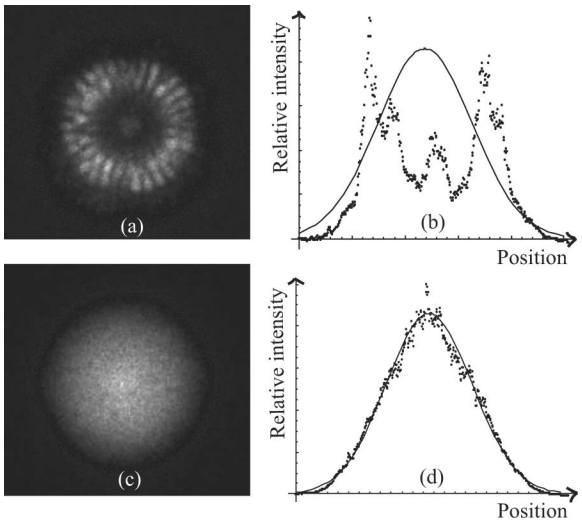

Fig. 6. FF intensity profile: above and below illustrate the modal and nonmodal case, respectively. The FF intensity distributions are shown in (a) and (c), and compared in (b) and (d) to a Gaussian fit as (4).

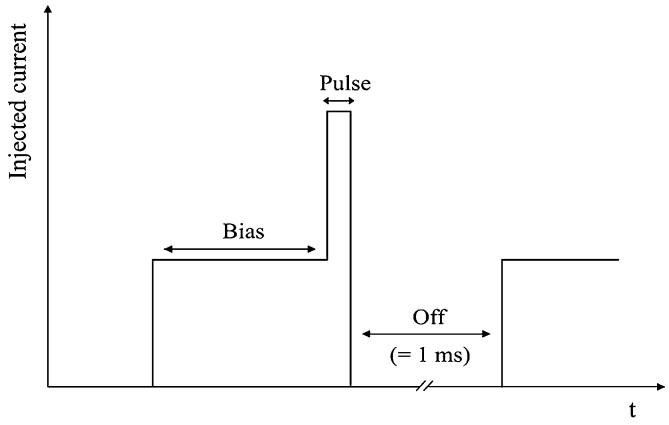

Fig. 7. Scheme of the electrical signal injected into the VCSEL consisting of a bias current pulse followed by a current pulse.

In order to objectively analyze our measurements, we first measure the FF intensity profile. A typical example of such a FF is shown in Fig. 6(a) for modal emission and in Fig. 6(c) for spatially incoherent emission. These FF profiles were measured using a slow nongated 12-bit CCD camera (*UP-680, Uniq Vision*) in order to have a large sensitivity and dynamic range. Next, we take a 1-D transverse cut through the center of the FF profile and fit this to a Gaussian function

$$G = D\ \exp -\frac{(x-av)^2}{2\sigma^2} \tag{4}$$

where x is the transverse (radial) position in the FF, av is the center position of the FF, and D is a scaling factor. In Fig. 6(b), we show a transverse cut of the modal FF pattern from Fig. 6(a) together with a fit to (4). Clearly, the FF profile does not resemble a Gaussian function. In the spatially incoherent emission regime, the FF profile has a Gaussian shape as can be seen in Fig. 6(d), where we compare the spatially incoherent emission pattern with a Gaussian fit.

We can, therefore, use the correlation between the measured FF profile and the corresponding Gaussian fit as a numerical indicator to quantify whether or not the VCSEL is emitting in the spatially incoherent emission regime. The correlation that we obtain for the modal emission in Fig. 6(b) is only 0.55, whereas the correlation resulting from Fig. 6(d) is 0.991. Based on a series of preliminary measurements, we have deduced that for fully developed spatially incoherent emission (i.e., no modal remnants are visible in the FF) the value of this Gaussian FF indicator should be larger than 0.99.

B. Thermal Lens Strength

In order to investigate the influence of the thermal lens on the appearance of spatially incoherent emission, we measure the Gaussian FF indicator for various strengths of the thermal lens. Therefore, we drive the VCSEL with electrical signals such as depicted in Fig. 7. We first send a bias current through the device for a certain amount of time. With this bias pulse, we install a thermal lens in the VCSEL prior to applying a current pulse that should drive the VCSEL into the incoherent emission regime. After the current pulse, we switch the VCSEL OFF for 1 ms in order to avoid thermal crosstalk between pulses. As discussed in Section III, we can change the thermal lens strength by varying the bias current. In this measurement, we want the resulting thermal lens to be fully developed before we apply the current pulse. From Figs. 3 and 4, we know that the thermal lens strength saturates after 7 μs. Therefore, we have chosen the bias length slightly larger, i.e., 10 μs.

The bias is followed by a current pulse through the device with an amplitude of 140 mA and a length that we vary from 100 ns to 1 μs. We then determine the value of the Gaussian FF indicator as a function of the pulse length for several bias amplitudes. A difficulty in our measurement procedure is that the FF profile contains a considerable modal contribution from the bias current. In order to eliminate this contribution such that we can access the effect of the injected pulse in the presence of a thermal lens, we use a differential analysis. We subtract the intensities of subsequent FF measurements, i.e., we subtract the FF measurement when only the bias is applied from the (bias + 100 ns pulse) FF measurement. Analogously, we subtract the (bias + 100 ns pulse) FF measurement from the (bias + 200 ns pulse) FF measurement, etc., in order to obtain the differential changes.

The result of this analysis is shown in Fig. 8 where we have plotted the Gaussian FF indicator versus the pulse length for different bias amplitudes. When no bias is applied and for small pulse lengths, we can see in Fig. 8 that the Gaussian FF indicator is low, indicating that the VCSEL's emission is modal. This holds for pulse durations up to 700 ns. For longer pulses, the indicator becomes larger than 0.99 and the VCSEL thus enters the spatially incoherent emission regime. If we increase the bias amplitude, the Gaussian FF indicator clearly increases and the pulse length after which the incoherent emission is attained decreases. When the bias is raised above 100 mA, we observe that the onset of spatially incoherent emission occurs immediately after turn-ON of the current pulse.

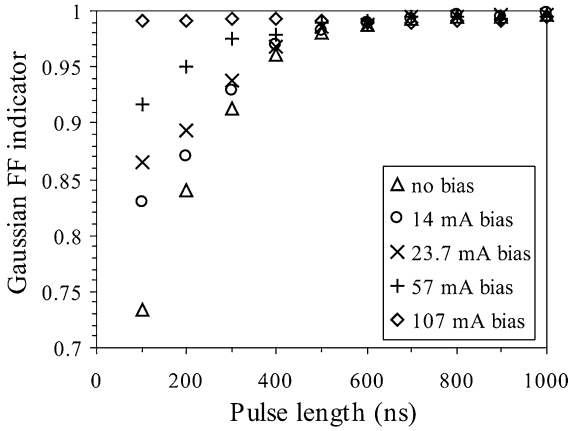

Fig. 8. Gaussian FF indicator as a function of pulse length. The different curves correspond to different bias amplitudes, varying from 0 to 107 mA.

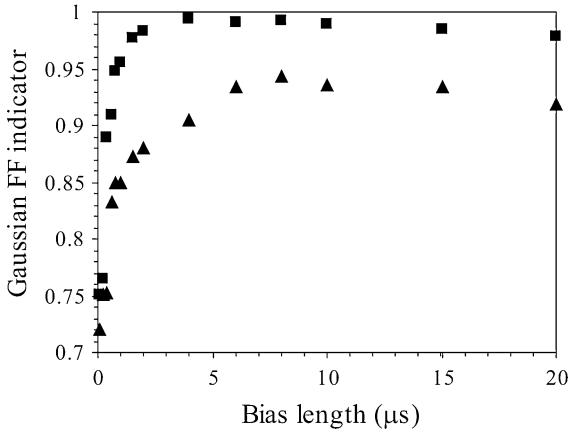

Fig. 9. Gaussian FF indicator as a function of the bias length. The triangles represent the result in case of a 57 mA bias level, the squares represent the result in case of a 90 mA bias level.

These measurements prove that the thermal lens needs to be sufficiently strong before spatially incoherent emission can occur. When no bias is applied, there is no thermal lens present in the beginning of the current pulse and the emission thus remains modal for short pulse lengths. For longer pulses (still without bias), the current pulse itself will gradually introduce a thermal lens in the device that finally leads to incoherent emission after 700 ns. When the bias is increased, the thermal lens present at the beginning of the current pulse will be enhanced, and hence, the pulse duration after which we observe spatially incoherent emission decreases.

C. Bias Length

The different roles of the thermal lens and the thermal chirp can be further evidenced by varying the length of the bias. In Fig. 3, the strength of the thermal lens increases up to about 7 μs, but remains almost constant for larger pulse lengths. Therefore, we are interested to know how the Gaussian FF indicator evolves for shorter or longer bias lengths. To this end, we measure the FF intensity for a bias current with fixed amplitude but a width varying from 1 to 20 μs, followed by a 100 ns pulse with the amplitude fixed at 140 mA. As the pulse length is relatively short compared to the bias length, we can assume that the thermal lens is only determined by the bias. Because of the fixed amplitude of the pulse, the thermal chirp during the 100 ns pulse will not change strongly when varying the bias length. However, for long bias lengths the heating during the bias will cause a slight decrease of the thermal chirp during the pulse. Nevertheless, this method allows us to separate the effect of the thermal lens from the effect of the thermal chirp.

From the FF measurements, we extract the value of the Gaussian FF indicator during the 100-ns-long pulse, which we have plotted in Fig. 9. We can see in Fig. 9 that for a 57 mA bias current the Gaussian FF indicator, being our measure for nonmodal emission, increases strongly up to about 7 μs. This indicates that, while the thermal chirp is kept at a constant rate, a more pronounced thermal lens drives the VCSEL more easily into the spatially incoherent emission regime. Installing a prebias for longer than 7 μs does not result in a further increase of the Gaussian FF indicator because the strength of the thermal lens does not increase any further.

As we observe the same timescale in the evolution of the thermal lens (see Fig. 3) as in the evolution of the Gaussian FF indicator (see Fig. 9), we conclude that the thermal lens plays a crucial role in establishing spatially incoherent emission.

In Fig. 9, we can also see that a bias current of 57 mA provides an insufficient thermal lens in order to induce spatially incoherent emission at the thermal chirp provided by a 100 ns pulse of 140 mA amplitude. A strong enough thermal gradient across the cavity can be ensured, however, for the 140 mA pulse in case of a preinstalled bias of 90 mA. For this bias level, the Gaussian FF indicator saturates close to 1 after a bias length of only 4 μs. For bias lengths larger than about 10 μs, we see that the Gaussian FF indicator decreases slightly, indicating a small modal contribution to the emission. Based on Figs. 3 and 4, we know that the thermal lens strength does not reduce at this timescale. This slight indicator decrease is rather due to a decrease of the thermal chirp rate for long bias lengths. These measurements prove that we need a minimum thermal lens profile and a specific chirp rate in order to drive the VCSEL in the spatially incoherent emission regime.

V. Minimum Chirp

In the previous paragraph, we have studied the thermal lens in the BA-VCSEL's cavity and the role it plays in inducing spatially incoherent emission. We now turn our attention to the other required thermal effect: thermal chirp. During the previous measurements, we chose to keep the thermal chirp rate high enough in order to be able to induce nonmodal emission in the presence of a sufficiently strong thermal lens. In the following paragraphs, we will report on measurements with varying pulse amplitudes, and thus, also varying chirp rate. The pulse length is consistently taken equal to 100 ns such that the pulse has a small influence on the thermal lens. In Fig. 10, we show the dependence of the Gaussian FF indicator on the pulse amplitude in case of a 4 μs bias for three different bias currents. For a bias current of 57 mA, the Gaussian FF indicator increases with increasing pulse amplitude or equivalently with increasing

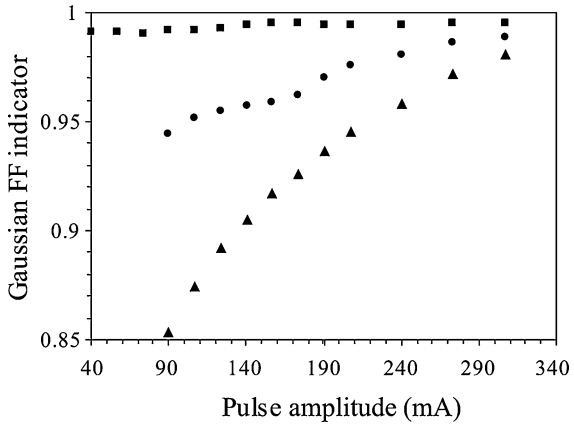

Fig. 10. Gaussian FF indicator as a function of the pulse amplitude. The three curves represent the results for three different bias currents: 57 mA (triangles), 74 mA (circles), and 90 mA (squares).

chirp rate during the pulse. But even at the maximum pulse amplitude, the 0.99 indicator threshold is not reached. For an increased bias current of 74 mA, the Gaussian FF indicator increases significantly because of the stronger thermal lens and the indicator crosses the 0.99 indicator threshold at a pulse amplitude of 310 mA. With a further increase of the bias current to 90 mA, the thermal lens is strong enough in order to induce nonmodal emission at a very low chirp rate. In this case, we observe spatially incoherent emission even for pulse amplitudes of 40 mA, for which the device clearly shows a modal emission pattern under continuous-wave (CW) driving conditions.

Based on these measurements, we can deduce the minimum chirp rate that is required to drive the VCSEL into the incoherent emission regime for various thermal lens strengths. The minimum chirp is determined by the current pulse amplitude for which the indicator goes from below to above 0.99. We have looked for this minimum pulse amplitude for various values of the bias amplitude and length. From the minimum pulse amplitude and its duration (which is 100 ns), we can use the derivative of (3) to calculate the corresponding chirp rate. In this derivation, we also take into account that the bias segment has already introduced some heating—and hence, thermal chirp—in the device. This effect will slightly reduce the chirp and thermal chirp rate compared to the situation when no bias pulse would be applied. The result of this measurement is shown in Fig. 11, where we plot the minimally required chirp rate for incoherent emission as a function of the thermal lens strength B. For values of B below 0.33, the maximum pulse amplitude of the electrical driver—and hence, the maximum chirp rate—is not high enough in order to drive the VCSEL into the incoherent emission regime. For a stronger thermal lens, the minimally required chirp strongly decreases with increasing lens strength. Based on these measurements, we can also derive an estimate of the MCBT. This is the time required for a coherent modal pattern to build up in the cavity. We assume that the spatially incoherent emission regime is reached once the chirp rate is sufficiently high as expressed by

$$\text{chirp rate} \geq \frac{\Delta\lambda}{\text{MCBT}} \tag{5}$$

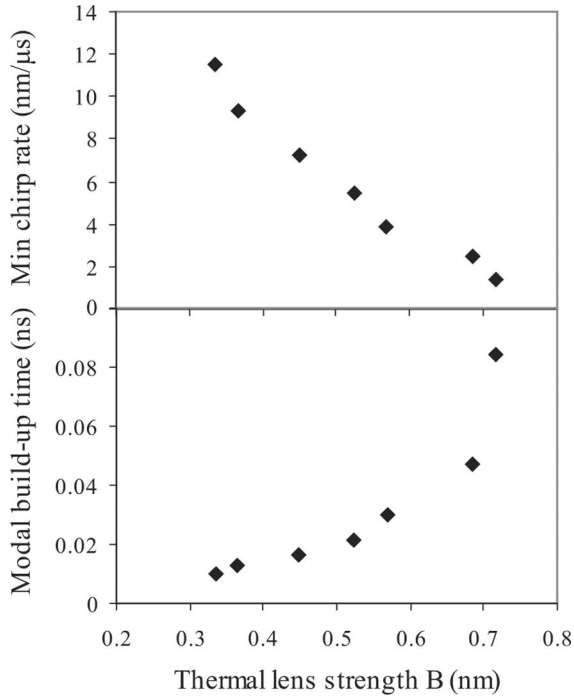

Fig. 11. Minimum chirp rate to reach the spatially in emission regime (top) and the modal build up top (bottom) as a function of the thermal lens strength.

where $\Delta\lambda$ is the linewidth of the mode. This equation expresses that modes will not have time to build up if we chirp the cavity by an amount larger than the linewidth of the mode during the time needed for the mode's coherence to build up. The linewidth of the different transverse modes is not easy to determine, but we can obtain a reasonable estimate of the linewidth by looking at the RF spectrum in CW operation. This RF spectrum consists of a large number of peaks [16] due to beating between the different transverse modes. The width of these beating peaks is related to the linewidth of the modes involved, leading to a measured estimate of the linewidth of about 50 MHz at an injection current of 80 mA. Neglecting any variations of the linewidth with mode number and output power, we can use (5) to estimate the MCBT as a function of the thermal lens strength. This is shown at the bottom of Fig. 11. The MCBT is a few picoseconds for a small thermal lens. For a lens strength B between 0.33 and 0.52, we observe a gradual increase of the MCBT. For larger values of B, the MCBT grows more rapidly. We were not able to determine the MCBT for a lens strength larger than 0.72 because the minimally required chirp rate becomes so small that we observe spatially incoherent emission for each value of the pulse amplitude. This is consistent with the measurement at a bias current of 90 mA in Fig. 10, for which the indicator stays above 0.99 for each value of the pulse amplitude. As the indicator does not cross the 0.99 threshold value, we cannot estimate the minimally required chirp and the MCBT at the corresponding lens strength B. Based on these measurements, we estimate that the MCBT increases to the nanoseconds range for large values of B. The measurements presented here are a first attempt in estimating the MCBT as a function of the thermal lens present in the VCSEL, and they will be complemented in

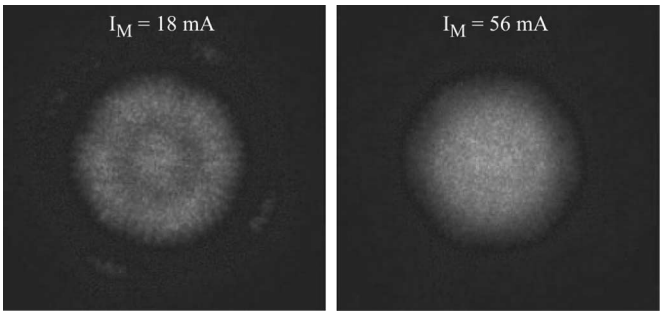

Fig. 12. FF intensity profile for a 500 KHz square wave modulation signal with an amplitude I_M of 18 mA (left) and 56 mA (right) added to a CW bias current of 70 mA.

the future by a more detailed experimental and theoretical study of the described phenomenon.

VI. Quasi CW

In our previous work, we have always employed pulses with a low duty cycle of typically 1% in order to generate spatially incoherent emission. The low duty cycle serves two purposes. First, it ensures that the VCSEL cools down before the next pulse is applied, such that the initial operating conditions are the same for each pulse. Second, the low duty cycle protects the VCSEL from overheating when we apply pulses with an amplitude much larger than the CW thermal rollover point. Notwithstanding the large peak output power during a pulse, the average emitted output power in the incoherent emission regime will be low because of the low duty cycle, which is disadvantageous for applications.

Based on the previous section we know that the pulse amplitude does not necessarily need to be large. If we can establish a strong thermal lens in the device, we are able to generate spatially incoherent emission at low pulse amplitudes. In that case, we can safely increase the duty cycle without risk of damaging the VCSEL. This is illustrated in Fig. 12 where we show the FF intensity profile for a square wave (i.e. duty cycle equal to 50%) modulated on top of a 70 mA CW bias current. Note that in this case we do not use a pre-bias segment in the current modulation signal. For small modulation amplitudes (see left image of Fig. 12) the value of the Gaussian FF indicator is 0.92 and we clearly see modal remnants in the FF profile. The thermal lens strength at 70 mA bias is not yet strong enough to establish spatially incoherent emission at a low chirp rate. When we increase the modulation amplitude to 56 mA (see image on the right of Fig. 12), the FF profile transforms into a Gaussian shape and the Gaussian FF indicator reaches a value of 0.993. At this modulation amplitude, the thermal lens and chirp rate are large enough to reach the spatially incoherent emission regime during the high amplitude segment of the square wave signal. During the square wave's time interval of low injection current, the injected current is lower than the VCSEL's threshold current and the re-appearance of modes (due to a gradually decreasing thermal lens) is suppressed. The square wave modulation signal drives the VCSEL beyond the CW thermal rollover, but since the modulation period is still small compared to thermal timescale (see upper graph in Fig. 5), this will result in only a small temperature rise during the high-amplitude segment of the square wave. As a result, the average output power at the modulation amplitude of 56 mA is the same as for the 18 mA square wave and is also equal to the CW output power at 70 mA. This way, we can generate a spatially incoherent beam with an average emitted output power of 60 mW.

VII. Conclusion

We have experimentally demonstrated that the spatially incoherent emission regime that can be invoked in BA-VCSELs stems from two different thermal effects: thermal lens and thermal chirp. We have separately measured the influence of these effects on the appearance of the spatially incoherent emission in BA-VCSELs. In order to separate these effects, we sent a current pulse through the device consisting of two segments. In a first segment, we sent a bias current through the VCSEL intended at generating a thermal lens in the device. Immediately after the bias, we sent an additional short pulse through the VCSEL that should drive the VCSEL in the incoherent emission regime. By means of a differential method, we measured the emission character only during the additional current pulse. Based on these measurements, we have shown that the incoherent emission regime sets on after a timescale corresponding to the build up of the thermal lens. A sufficiently strong thermal lens has to be present in order to increase the time needed for the coherence of a mode to build up. Once this modal coherence buildup time is large enough, thermal chirp prevents the formation of modes and the VCSEL emits a spatially incoherent beam. We demonstrated that the required chirp rate during the pulse strongly depends on the strength of the thermal lens. We have proven that it is possible to obtain spatially incoherent emission even at low-pulse amplitudes and/or large duty cycles provided that a large thermal lens or refractive index gradient is present in the VCSEL.

Acknowledgment

The authors are indebted to M. Grabherr of U-L-M Photonics GmbH for providing excellent BA-VCSELs and Wolfgang Elsäßer for valuable support and discussions.

References

[1] C. Wilsen, H. Temkin, and L. A. Coldren, *Vertical-Cavity Surface-Emitting Lasers: Design, Fabrication, and Applications*. New York: Cambridge Univ. Press, 1999.

[2] F. Koyama, "Recent advances of VCSEL photonics," *J. Lightw. Technol.*, vol. 24, no. 12, pp. 4502–4513, Dec. 2006.

[3] A. W. Jackson, R. L. Naone, M. J. Dalberth, J. M. Smith, K. J. Malone, D. W. Kisker, J. F. Klem, K. D. Choquette, D. K. Serkland, and K. M. Geib, "OC-48 capable InGaAsN vertical cavity lasers," *Electron. Lett.*, vol. 37, pp. 355–356, 2001.

[4] J. Boucart, G. Suruceanu, P. Royo, V. I. Iakovlev, A. Syrbu, A. Caliman, A. Mereuta, A. Mircea, C.-A. Berseth, A. Rudra, and E. Kapon, "3.125-Gb/s modulation up to 70 degrees Celsius using 1.3 micrometer VCSELs fabricated with localised wafer fusion for 10GBASE LX4 applications," *IEEE Photon. Technol. Lett.*, vol. 18, no. 4, pp. 571–573, Feb. 2006.

[5] E. Mohammed, A. Alduino, T. Thomas, H. Braunisch, D. Lu, J. Heck, A. Liu, I. Young, B. Barnett, G. Vandentop, and R. Mooney, "Optical interconnect system integration for ultra-short-reach applications," *Intel Technol. J.*, vol. 8, pp. 115–127, 2004.

[6] W. W. Bewley, C. L. Felix, I. Vurgaftman, E. H. Aifer, L. J. Olafsen, J. R. Meyer, L. Goldberg, and D. H. Chow, "Mid-infrared

vertical-cavity surface-emitting lasers for chemical sensing," *Appl. Opt.*, vol. 38, pp. 1502–1506, 1999.
[7] E. Thrush, O. Levi, W. Ha, G. Carey, L. J. Cook, J. Deich, S. J. Smith, W. E. Moerner, and J. S. Harris, "Integrated semiconductor vertical-cavity surface-emitting lasers and PIN photodetectors for biomedical fluorescence sensing," *IEEE J. Quantum Electron.*, vol. 40, no. 5, pp. 491–498, May 2004.
[8] J. Ostermann, F. Rinaldi, P. Debernardi, and R. Michalzik, "VCSELs with enhanced single-mode power and stabilized polarization for oxygen sensing," *IEEE Photon. Technol. Lett.*, vol. 17, no. 11, pp. 2256–2258, Nov. 2005.
[9] A. Haglund, J. Gustavsson, J. Vukusic, P. Modh, and A. Larsson, "Single fundamental-mode output power exceeding 6 mW from VCSELs with a shallow surface relief," *IEEE Photon. Technol. Lett.*, vol. 16, no. 2, pp. 368–370, Feb. 2004.
[10] H. J. Unold, S. W. Z. Mahmoud, R. Jager, M. Grabherr, R. Michalzik, and K. J. Ebeling, "Large-area single-mode VCSELs and the self-aligned surface relief," *IEEE J. Sel. Topics Quantum Electron.*, vol. 7, no. 2, pp. 386–392, Mar./Apr. 2001.
[11] J. G. McInerney, A. Mooradian, A. Lewis, A. V. Shchegrov, E. M. Strzelecka, D. Lee, J. P. Watson, M. Liebman, G. P. Carey, B. D. Cantos, W. R. Hitchens, and D. Heald, "High-power surface emitting semiconductor laser with extended vertical compound cavity," *Electron. Lett.*, vol. 39, pp. 523–525, 2003.
[12] M. Miller, M. Grabherr, R. King, R. Jäger, R. Michalzik, and K. J. Ebeling, "Improved output performance of high-power VCSELs," *IEEE J. Sel. Topics Quantum Electron.*, vol. 7, no. 2, pp. 210–216, Mar./Apr. 2001.
[13] C. J. Chang-Hasnain, M. Orenstein, A. Von Lehmen, L. T. Florez, J. P. Harbison, and N. G. Stoffel, "Transverse mode characteristics of vertical cavity surface-emitting lasers," *Appl. Phys. Lett.*, vol. 57, pp. 218–220, 1990.
[14] C. Degen, I. Fischer, and W. Elsäßer, "Transverse modes in oxide confined VCSELs: Influence of pump profile, spatial hole burning, and thermal effects," *Opt. Exp.*, vol. 5, pp. 38–47, 1999.
[15] M. Peeters, G. Verschaffelt, H. Thienpont, S. K. Mandre, I. Fischer, and M. Grabherr, "Spatial decoherence of pulsed broad-area vertical-cavity surface-emitting lasers," *Opt. Exp.*, vol. 13, pp. 9337–9345, 2005.
[16] S. K. Mandre, W. Elsäßer, I. Fischer, M. Peeters, and G. Verschaffelt, "Evolution from modal to spatially incoherent emission of a broad-area VCSEL," *Opt. Exp.*, vol. 16, pp. 4452–4464, 2008.
[17] L. Mandel and E. Wolf, *Optical Coherence and Quantum Optics*. Cambridge, U.K.: Cambridge Univ. Press, 1995.
[18] A. C. Schell, "A technique for the determination of the radiation pattern of a partially coherent aperture," *IEEE Trans. Antennas Propag.*, vol. AP-15, no. 1, pp. 187–188, Jan. 1967.
[19] F. Riechert, G. Craggs, Y. Meuret, B. Van Giel, H. Thienpont, U. Lemmer, and G. Verschaffelt, "Low speckle laser projection with a broad-area vertical-cavity surface-emitting laser in the nonmodal emission regime," *Appl. Opt.*, vol. 48, pp. 792–798, 2009.
[20] Y.-G. Zhao and J. G. McInerney, "Transient temperature response of vertical-cavity surface-emitting semiconductor lasers," *IEEE J. Quantum Electron.*, vol. 31, no. 9, pp. 1668–1673, Sep. 1995.
[21] J. Chen, A. Hangauer, and M.-C. Amann, "Simplified model of the dynamic thermal tuning behavior of VCSELs," *IEEE Photon. Technol. Lett.*, vol. 20, no. 13, pp. 1082–1084, Jul. 2008.
[22] S. K. Mandre, W. Elsäßer, I. Fischer, M. Peeters, and G. Verschaffelt, "Determining the temporally and radially resolved temperature distribution inside a pulsed broad-area vertical-cavity surface-emitting laser cavity," *Appl. Phys. Lett.*, vol. 89, pp. 151106-1–151106-3, 2006.
[23] G. Verschaffelt, G. Craggs, M. Peeters, S. Mandre, H. Thienpont, and I. Fischer, "Spatially resolved characterization of the coherence area in the incoherent emission regime of a broad-area vertical-cavity surface-emitting laser," *IEEE J. Quantum Electron.*, vol. 45, pp. 249–255, Mar. 2009.

Gordon Craggs was born in Ukkel, Belgium, in 1985. He received the M.Sc. degree in physics from Vrije Universiteit Brussel (VUB), Brussels, Belgium, in June 2007, where he is currently working toward the Ph.D. degree.

His current research interests include coherence properties of semiconductor lasers, and is currently engaged in broad-area vertical-cavity surface-emitting lasers.

Guy Verschaffelt (M'99) was born in Belgium, in 1973. He received the M.E. degree in photonics and the Ph.D. degree from the Vrije Universiteit Brussel (VUB), Brussels, Belgium, in 1996 and 2000, respectively.

He is currently a Postdoctoral Researcher with VUB. His current research interests include polarization and noise properties of vertical-cavity surface-emitting lasers and microchip Nd:YAG lasers, emission properties of broad-area high-power semiconductor lasers, and the study of semiconductor ring lasers.

Shyam K. Mandre was born in Frankfurt, Germany, in 1977. He received the Diploma degree in physics and the Ph.D. degree from Darmstadt University of Technology, Darmstadt, Germany, in 2002 and 2006, respectively.

He is currently with the R&D Department, Procter and Gamble/Braun GmbH, Kronberg, Germany. His current research interests include the control of the spatiotemporal emission dynamics and spectral emission properties of both, broad-area lasers and multi-mode VCSELs, as well as on the coherence properties of large-area vertical-cavity surface-emitting lasers (VCSELs).

Hugo Thienpont (M'97) was born in Ninove, Belgium, in 1961. He graduated in electrotechnical engineering and received the Ph.D. degree in applied sciences from the Vrije Universiteit Brussel (VUB), Brussels, Belgium, in 1984 and 1990, respectively.

In 1994, he became a Professor at the Faculty of Applied Sciences, where he was engaged in teaching photonics. In 2000, he became a Research Director of the Department of Applied Physics and Photonics, VUB, and in 2004, he was elected the Chair of the department. Currently, he is the coordinator of several basic research and networking projects such as the European Network of Excellence on Micro-Optics (NEMO).

Prof. Thienpont is a Fellow Member of the International Society for Optical Engineering (SPIE) and Electrical Optical Systems (EOS), and a member of Optical Society of America (OSA) and IEEE Laser & Electro-Optics Society (LEOS).

Ingo Fischer received the Diploma and Ph.D. degrees in physics from the Philipps University, Marburg, Germany, in 1992 and 1995, respectively.

After finishing his doctoral work, he was with Darmstadt University of Technology, Darmstadt, Germany, from 1995 to 2004. From 2005 to 2007, he was with Vrije Universiteit Brussel (VUB), Brussels, Belgium. Since 2007, he has been a Full Professor in photonics with Heriot-Watt University, Edinburgh, U.K. His studies are focused on nonlinear photonics and brain dynamics. In particular, he is concentrating on emission properties and dynamics of modern photonic sources, coupled laser systems, synchronization of lasers and neurons, and utilization of chaos.

Dr. Fischer was the recipient of the Research Prize of the Adolf-Messer Foundation in 2000 and the first Hassian Cooperation Prize of the Technology Transfer Network in 2004.